X-ray Diffraction and Molecular Simulation Study of the Crystalline and Liquid States of Succinic Anhydride

Valeria Ferretti,[a] Paola Gilli,[a] and Angelo Gavezzotti*[b]

Abstract: The crystal structure of succinic anhydride was studied at five temperatures between 100 K and the melting point by single-crystal X-ray diffraction. The temperature dependence of molecular libration tensors was determined. Intermolecular interactions, in particular through unusually close molecule–molecule contacts, are discussed, with a detailed calculation of electrostatic energies. A method for the adaptation of existing crystal force fields to molecular dynamics has been developed; the adapted force field was used to study molecular motion and rotational diffusion with increasing temperature. Equilibration of the crystalline system becomes impossible at a temperature very close to the experimental melting temperature, where a sudden transition to the liquid state occurs, and a partial kinetic picture of the melting process is obtained. After validation of the force field against experimental crystal data, the state equation of the liquid was predicted. Enthalpies of sublimation, melting, and vaporization were calculated. The dynamics of a solution of succinic anhydride in a nonpolar solvent was simulated, for a discussion of the aggregation process leading to demixing and to crystal nucleation.

Keywords: molecular dynamics · organic crystals · phase transitions · solid-state structures · X-ray diffraction

Introduction

In the last few decades, single-crystal X-ray diffraction on organic crystals has provided a detailed picture of crystal architecture and packing, and the Cambridge Structural Database[1] (CSD) now has extensive facilities for the analysis of intermolecular geometry. However, it is seldom remembered that this picture results from time-averaging over molecular librations and has a deceptively static character. Dynamic aspects of crystal packing have been much less considered, and little effort has been devoted to studies of the thermal dependence of intermolecular parameters; the dynamic information obtainable from X-ray atomic displacement parameters is, at best, indirect; the theory and practice of librational tensors has been recently revisited by Burgi et al.[2] In traditional crystallography, which aims at molecular geometries, it is not surprising that most studies on temperature dependence have been dedicated to low temperatures, where molecular motion is quenched; the number of crystal structures in the CSD that were determined above room temperature is estimated at less than 0.1 %. In the perspective of a structural and energetic study of the properties of materials and of their phase behavior, more effort should instead be devoted to high-temperature studies, in which the relevant phenomenon of molecular motion is enhanced, even at the price of a loss of resolution. However, X-ray diffraction on organic crystals above room temperature is still sporadic, due to both lack of interest and experimental difficulties, even though X-ray diffractometers have been developed to the point that a full crystal structure determination is a matter of a few hours, and temperature control is no longer such a severe problem.

Much progress in the field of the phase behavior of organic substances is expected from theoretical studies. Lattice dynamics allows an evaluation of crystal free energies, although in its traditional form it is restricted to the harmonic approximation. Recently, attempts were made to overcome this obstacle, with a full molecular dynamics (MD) treatment,[3, 4] which becomes increasingly necessary as the temperature is raised toward the melting point. In fact, molecular dynamics is by now a fully affordable method in crystal structure analysis[5, 6] and in the study of phase transitions.[7–8]

We use a combination of theoretical and experimental methods to investigate molecular properties and intermolecular energies and forces in a variable-temperature regime, from the zero-point energy limit up to as close as possible to the melting temperature. Herein we report: 1) an analysis of temperature-dependent crystal structure and thermal libration parameters from single-crystal X-ray diffraction; 2) the calculation of electrostatic energies in the crystal structure; 3)

[a] Prof. V. Ferretti, Prof. P. Gilli
Dipartimento di Chimica, Università di Ferrara
via Borsari 46, Ferrara (Italy)

[b] Prof. A. Gavezzotti
Dipartimento di Chimica Strutturale e Stereochimica Inorganica
Università di Milano, via Venezian 21, 20133 Milano (Italy)
Fax: (+39) 02-70635288
E-mail: angelo.gavezzotti@unimi.it

  0947-6539/02/0807-1710 $ 20.00+.50/0

molecular dynamics simulations of the state equation of the solid, analysis of pre-melting phenomena, and simulation of melting; 4) prediction of the state equation of the liquid by molecular dynamics; 5) molecular dynamics simulations of the very first steps of nucleation from nonpolar solvents. The molecular mechanism of melting of organic crystals has seldom been studied, and apparently has never been explained (see refs.[9, 10], and discussions therein). This is even more true for the reverse process of crystal nucleation.[11–12]

Succinic anhydride was chosen as test molecule for this case study because a) it is a nearly ideal object for theoretical studies: small, rigid, and with a possibility for reliable parameterization of the intermolecular force field; and b) it is a cheap and stable chemical that is sufficiently high melting to allow easy handling at and above ambient temperature.

Experimental Section

Succinic anhydride was purchased from Aldrich and recrystallized from hot chloroform as large white needles. Recrystallization from THF, chloroform, or acetonitrile yielded the same crystal form, as confirmed by repeated powder diffraction patterns. Differential scanning calorimetry (DSC) confirmed a melting point of 392–393 K and the specific heat of the crystal at 298 K (see below). No pre-melting features appeared in the DSC trace.

Single-crystal diffraction data were collected at 100, 150, 225, 295, and 353 K, and no significant difficulties were encountered in temperature control in this range. Diffraction data were collected on a Nonius Kappa diffractometer equipped with a CCD detector and an Oxford Cryosystem cooling apparatus with graphite-monochromatized $Mo_{K\alpha}$ radiation ($\lambda =$ 0.71069 Å). Intensities were corrected for Lorentz and polarization effects. The structure was solved by direct methods with the SIR92 suite of programs,[13] and refinements were performed on F^2 by full-matrix least-squares methods (SHELX97[14]). The H atoms were located in difference Fourier maps and refined isotropically. All other calculations, includig rigid-body analysis, were performed by PLATON[15] and WingX.[16]

Data collection and refinement parameters: space group $P2_12_12_1$, orthorhombic, $Z = 4$; for cell parameters see Table 1. 100 K: $\mu = 0.138\,mm^{-1}$, $\theta_{max} = 41.5^\circ$. Of 1638 unique measured reflections, 1561 with $I > 2\sigma(I)$ were used in the refinement. $R = 0.0295$ (on F^2), $R_w = 0.0789$. 150 K: $\mu =$ $0.137\,mm^{-1}$, $\theta_{max} = 30.1^\circ$. Of the 755 unique measured reflections, 731 with $I > 2\sigma(I)$ were used in the refinement. $R = 0.0259$ (on F^2), $R_w = 0.0640$. 225 K: $\mu = 0.135\,mm^{-1}$, $\theta_{max} = 32.5^\circ$. Of the 859 unique measured reflections, 801 with $I > 2\sigma(I)$ were used in the refinement. $R = 0.0333$ (on F^2), $R_w = 0.0846$. 295 K: $\mu = 0.132\,mm^{-1}$, $\theta_{max} = 30.0^\circ$.Of the 776 unique measured reflections, 738 with $I > 2\sigma(I)$ were used in the refinement. $R = 0.0359$ (on F^2), $R_w = 0.0935$. 353 K: $\mu = 0.130\,mm^{-1}$, $\theta_{max} = 29.6^\circ$. Of the 709 unique measured reflections, 561 with $I > 2\sigma(I)$ were used in the refinement. R (on F^2) $= 0.0631$ $R_w = 0.2132$. CCDC-171946–171950 contain the supplementary crystallographic data for this paper. These data can be obtained free of charge via www.ccdc.cam.ac.uk/conts/retrieving.html (or from the Cambridge Crystallographic Data Centre, 12 Union Road, Cambridge CB2 1EZ, UK; fax: (+44) 1223-336-033; or deposit@ccdc.cam.uk).

Methods of Calculation

The GROMOS96 program package[7] was used, but the force field was parameterized ex novo. In all MD calculations reference molecular dimensions were taken from the X-ray geometry at 295 K, with hydrogen atom positions re-normalized at C–H 1.08 Å. For a small, rigid molecule like succinic anhydride the intramolecular part of the force field is not so crucial: bond stretching was quenched by the SHAKE approximation,[18] while bending potentials and improper torsion restraints were applied mainly to prevent large deformations and deviations from planarity, as in previous work.[7, 12]

The intermolecular part of the force field (FF) is crucial for our purposes. Two starting points for the optimization of intermolecular interaction parameters for succinic anhydride were considered, namely, OPLS-FF[19, 20] and UNI-FF.[21, 22] The OPLS-FF has no special terms for anhydrides, so adaptation of parameters used for succinic acid[19] was considered: for $E = 4\,\varepsilon[(\sigma/r)^{12} - (\sigma/r)^6]$, $\sigma(i,j) = [(\sigma(i)\sigma(j)]^{1/2}$, $\varepsilon(i,j) = [\varepsilon(i)\varepsilon(j)]^{1/2}$, charge, σ and ε [kJ mol^{-1}] were assigned as: carbonyl C, 0.550, 3.750, 0.439 (as carbonyl C in esters); carbonyl O, −0.450, 2.960, 0.879 (as carbonyl O in esters); methylene C, −0.120, 3.500, 0.276; methylene H, 0.060, 2.500, 0.126; –O–, −0.400, 3.000, 0.711 (–O– in esters) or −0.400, 2.900, 0.589 (–O– in ethers).

Systematic tests were conducted with these tentative intermolecular parameters, but the results for crystal density and lattice energy were not satisfactory. Far from implying a malfunction of the OPLS force field, this lack of success was probably due to the many approximations involved, also because the GROMOS96 architecture is not entirely compatible with certain forms of the OPLS parameterization. A different strategy was then adopted.

The UNI potentials, originally given in the form $E = A\exp(-BR) - CR^{-6}$, were recast in the 12-6 functional form used by the MD programs. These chargeless potentials, calibrated for a wide variety of organic crystals, are known[21] to fail in reproducing some of the critical features of the crystal packing of succinic anhydride, which exhibits strong interactions between atoms of different electronegativity (see below). Also, previous experience showed that for use in dynamic simulations the steepness of the repulsive part of the potentials must be reduced. The UNI potentials were therefore supplemented by the introduction of charge parameters and R^{-1} terms, and rescaled by reducing the equilibrium distance σ and by slightly increasing the depth of the potential well ε. After several tests, a 3% rescaling ($\varepsilon' = 1.03\,\varepsilon$ and $\sigma' = 0.97\,\sigma$) was found to give the best results. Note that a 1% change in these parameters has a substantial effect on performance. The OPLS charges[19] were used as a guideline, but slight rearrangements were necessary for keeping the anhydride group and each methylene group neutral, to comply with the charge-group procedure in GROMOS96.[18] The final optimized parameters, calibrated to reproduce enthalpies of sublimation and densities at room temperature, are collected in Table 2. The heat of sublimation was calculated at 295 K, as in previous work, by taking the sum of electrostatic and van der Waals potential energies and adding 3% to account for the lack of convergence due to the summation cutoff, to be 79.6 kJ mol^{-1} (30% coulombic), which compares to an experimental value of 80.7 kJ mol^{-1} at 298 K.[23] The calculated crystal density at 295 K for a box volume of 26.712(97) nm^3 is 1.493 g cm^{-3}

Table 1. Crystal data for succinic anhydride.[a]

T/K	a [Å]	b [Å]	c [Å]	ρ [g cm^{-3}]	Shortest d(C···O) [Å]		d(C···O) [Å]
					S_y	S_x	
100	5.3548(1)	6.8163(2)	11.5628(3)	1.575	2.94	3.03	3.03
150	5.3696(2)	6.8471(2)	11.5935(3)	1.559	2.96	3.04	3.04
225	5.3947(1)	6.9068(2)	11.6491(3)	1.531	2.99	3.07	3.07
295	5.4257(2)	6.9746(2)	11.7167(3)	1.499	3.02	3.11	3.10
353	5.4435(4)	7.0293(5)	11.7550(13)	1.478	3.04	3.14	3.13

[a] See text for definition of S_y and S_x.

Table 2. Parameters[a] for $E_{ij}(\text{atom}-\text{atom}) = AR_{ij}^{-12} - BR_{ij}^{-6} + (q_iq_j)R_{ij}^{-1}$ in the final force field.

	$10^6 A$	$10^3 B$	q
H···H	0.06263	0.10396	H: +0.10
H···C	0.24035	0.45100	–
H···O	0.08416	0.41845	–
C···C	3.3329	2.3064	C: +0.50 (C=O), −0.20 (CH_2)
C···O	2.3574	2.5578	–
O···O	1.1708	1.2742	O: −0.375 (C=O), −0.25 (ether)
CCl_4[b]	6460.0	324.5	–

[a] R is an intermolecular interatomic distance [Å], E is in kJ mol^{-1}. Charges in electrons. [b] Usual square-root combination rules were used for interaction parameters between solvent and other atomic species.

(experimental room-temperature value 1.499 g cm^{-3}). There is no straightforward way of estimating the C_p(crystal) from the results of our MD simulations for comparison with experiment (110.9 J K^{-1} mol^{-1}[24]).

Molecular dynamics (MD) calculations were performed in an NPT ensemble (constant number of particles, pressure, and temperature), with periodic boundary conditions: the coupling constants were 0.1 and 0.5 ps for T and isotropic P, respectively. Energy summations were extended to a cutoff of 11 Å, convergence problems in coulombic interactions being mitigated by the charge-group approach. Extensive tests with reaction field corrections[25] and checking against calculations with Ewald sums[26] showed that this convergence criterion is realistic. The integration step was 2 fs.

For simulations on pure crystal and pure liquid, the computational box contained 240 molecules from $5 \times 4 \times 3$ crystal unit cells (box dimensions at 300 K were 27.2, 27.9, and 35.2 Å, that is, well above twice the cutoff radius). The crystal–liquid phase transition was simulated by a stepwise increase in temperature from 100 to 420 K, each temperature being held long enough to allow full equilibration (100–200 ps in the 100–300 K interval, and up to 300 ps for the higher temperatures in the liquid state). The temperature step was 5 K in the crucial 390–420 K range. The last frame at each T was taken as the starting frame for the $T + \Delta T$ run.

For the simulations in solution, a cubic computational box was prepared from an equilibrated box of 2196 united-atom CCl_4 solvent molecules (sides of 69.71 Å) by substituting at random 51 solute succinic anhydride molecules in place of the same number of solvent molecules. The united-atom solvent parameters[27] were merged with those of the solute by the usual mixing rules (see Table 2). In the starting configuration of the solution computational box, molecules were placed as far apart as possible, and only one distance between molecular centers of coordinates was smaller than 7 Å. Energy minimization cycles were first performed to dispose of a number of hard repulsive contacts in the initial configuration. The output of this minimization was used as input for a startup MD run at 200 K, assigning Boltzmann velocities, and then for warm-up cycles at 250, and finally for production runs at room temperature (298 K) for 4.5 ns. Alternatively, dimers or trimers extracted from the crystal structure along what were thought to be special interaction directions were solvated in the same solvent box and simulated at room temperature for variable time intervals.

Results

X-ray crystal structure analysis and lattice energies: This work confirmed the previous[28] assignment of the space group. Crystal data are summarized in Table 1, and molecular parameters in Table 3. Figure 1 shows ORTEP[29] plots of the atomic displacement parameters (ADPs) as a function of temperature, as well as the atom-numbering scheme.

Table 3. Molecular data for succinic anhydride.

T [K]	Vibrational C_v [J K^{-1} mol^{-1}]	av d(C–O) [Å]	av d(C=O) [Å]	max. Δ[a] [Å]	min.–max. rbc[b] [Å]
100	17.2	1.3863(3)	1.1985(3)	0.020	0.003–0.006
150	27.5	1.3863(8)	1.1932(13)	0.020	0.005–0.009
225	48.4	1.3848(4)	1.1898(6)	0.017	0.008–0.014
295	70.5	1.382(1)	1.188(3)	0.014	0.011–0.019
353	85.0	1.377(3)	1.182(3)	0.010	0.015–0.025

[a] Maximum distance of an atom from the mean molecular plane. [b] rbc = Rigid-body correction.

The succinic anhydride crystal is very stable and immutable in the whole 100–353 K range, as confirmed by crystallization of the same form from different solvents, by the absence of special features in the thermograms, and by the smooth evolution with temperature of all X-ray crystal structure parameters. This is one case in which the existence of polymorphs under ambient conditions can be confidently ruled out. The relatively small difference in heat capacity between gas and crystal (12 J K^{-1} mol^{-1} at 298 K)[23, 24] points

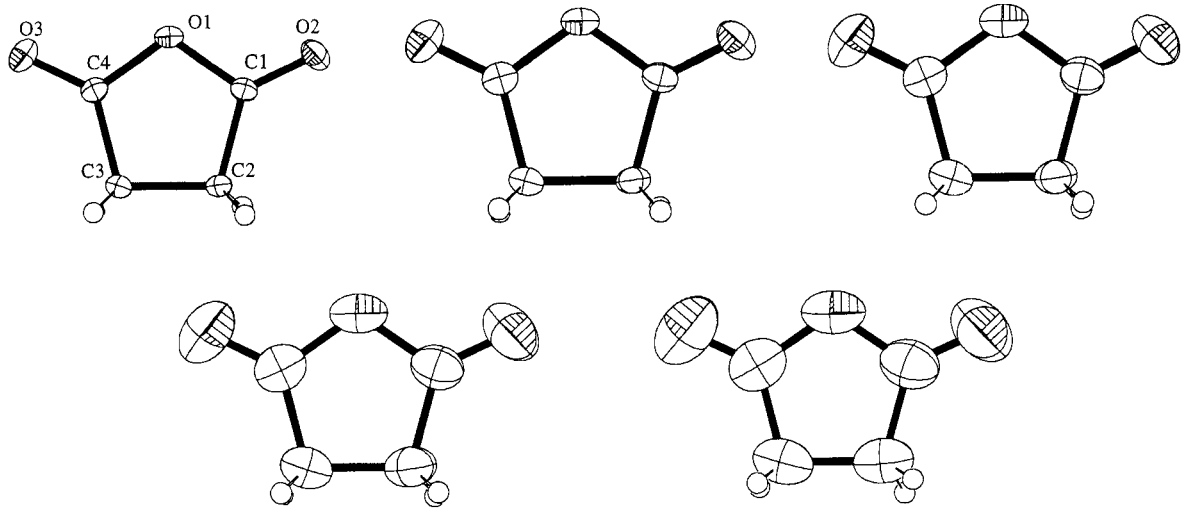

Figure 1. Atom numbering and ORTEP plots at 50% probability level at the five temperatures of Table 1.

0947-6539/02/0807-1712 $ 20.00+.50/0 *Chem. Eur. J.* **2002**, *8*, No. 7

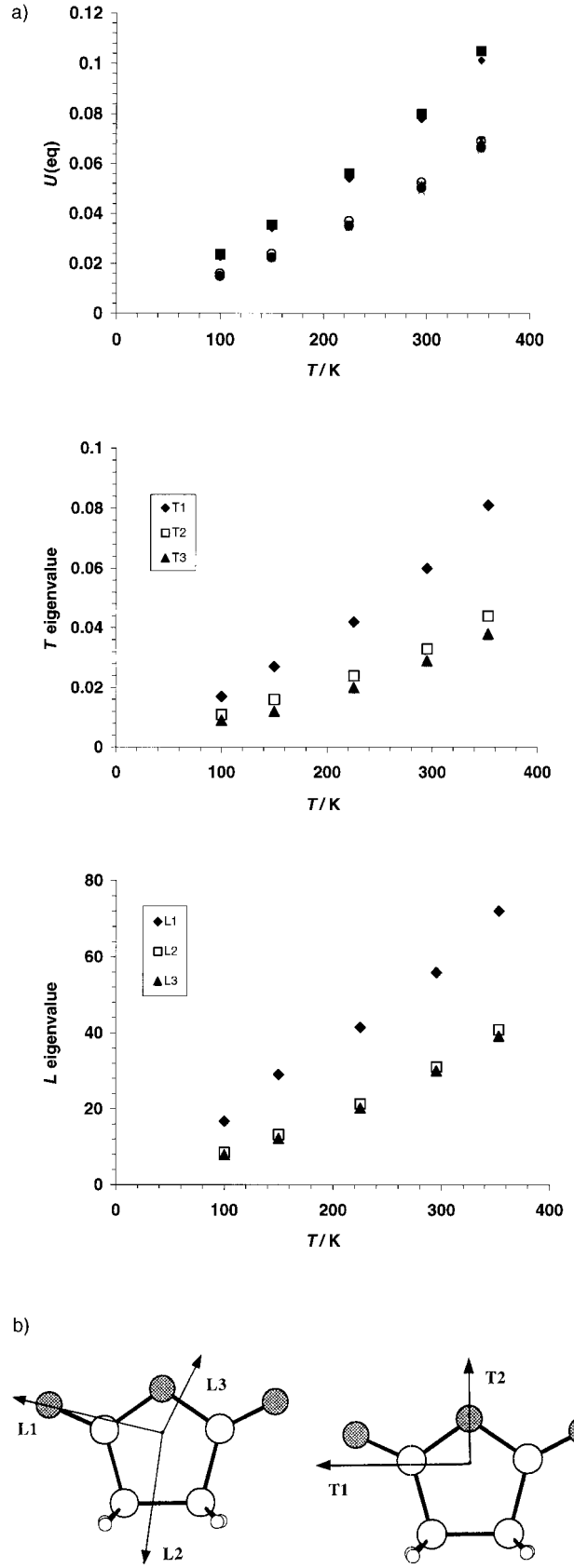

Figure 2. a) Top to bottom: plot of U_{eq} [Å^2] for carbonyl O atoms (upper symbols) and ring atoms (lower symbols); translational tensor eigenvalues [Å^2]; librational tensor eigenvalues [deg^2], as a function of temperature. b) Axis labeling and directions.

to the existence of rather strong crystal forces that result in high-frequency lattice vibrations.

The thermal expansion (see Table 1) is moderately anisotropic, the coefficient along the cell axis b ($1.2 \times 10^{-4}\,K^{-1}$) being about twice that along a and c. Figure 2a shows the temperature dependence of the equivalent ADP U_{eq} of each non-hydrogen atom in the molecule: the carbonyl oxygen atoms have a much larger ADP than other atoms. Figure 2a also shows the temperature dependence of the eigenvalues of the translational and librational tensors, respectively. Figure 2b shows the axis directions.

Data in Table 3 confirm that the succinic anhydride molecule is essentially a rigid body at all temperatures, with little or no deviation from planarity. The gas-phase vibrational heat capacities $C_{v,vib}$ at different temperatures were obtained by frequency calculations on the fully optimized geometry at the B3LYP/6-31 + G(d,p)//B3LYP/6-31 + G(d,p) level[30] (experimental and optimized distances: C–O 1.386 – 1.391, C=O 1.198 – 1.197, C–C 1.501 – 1.521, C–C 1.525 – 1.531 Å). The predicted heat capacity ($C_p = (C_{v,vib} + 3R) + R =$ 103.8 J K^{-1} mol^{-1}) compares with a literature value of 98.0 J K^{-1} mol^{-1} at 302 K.[24] Interestingly, two intramolecular vibrational modes—methylene rocking at 47 cm^{-1} and a "butterfly" motion of the carbonyl oxygen atoms at 141 cm^{-1}—may in principle be allowed to mix into the external lattice modes.

Further data for the interpretation of the packing of succinic anhydride can be gathered by considering the first coordination shell of the molecule in the crystal, which includes eight closest neighbor molecules (Table 4): two molecules along each of the three screw axes (labeled S_x, S_y, S_z), and two molecules translated along the shortest cell axis (labeled T_x). A recognizable molecular interlocking pattern in the succinic anhydride crystal (Figure 3) includes nesting of the two carbonyl oxygen atoms against the molecular rings of two neighbor molecules (S_y and S_x) with particularly short C=O ··· C=O contacts, almost an incipient nucleophilic attack; the shortest O ··· C contact distance stretches from 2.94 Å at 100 K to 3.04 Å close to the melting point. At room temperature, the two short O ··· C contact distances are 3.02 and 3.11 Å, well below the sum of any reasonable atomic radii. The thermal evolution of atomic displacement parameters (Figure 2) is not inconsistent with the picture in Figure 3: molecular motions (L1 libration and T1 translation) that are less disruptive of the tight intermolecular pattern increase more steeply with increasing temperature.

Table 4. For the four molecular pairs around the succinic anhydride molecule in the crystal (see text for definitions): distance between molecular centers of mass [Å] and angles between molecular planes [°]. Molecule – molecule electrostatic potential interaction energies E in kJ mol^{-1} at 150 K.

T/K	S_x distance	angle	S_y distance	angle	T_x distance	S_z distance	angle
100	4.42	62	4.65	82	5.35	6.11	48
150	4.43	61	4.67	82	5.37	6.12	49
225	4.45	61	4.71	82	5.39	6.16	49
295	4.48	60	4.75	82	5.433	6.19	50
353	4.50	60	4.78	83	5.44	6.21	51
E	– 4.1		– 21.9		– 11.8	– 16.0	

  0947-6539/02/0807-1713 $ 20.00+.50/0

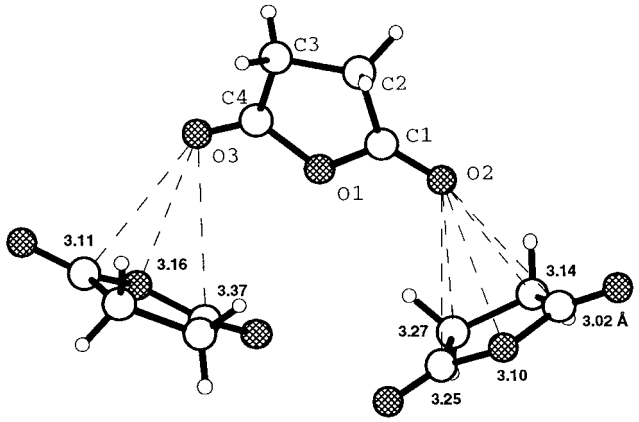

Figure 3. A strong molecular interaction motif in the succinic anhydride crystal: the molecule at the top interacts with an S_x-related molecule (left) and an S_y-related molecule (right). C···O and O···O distances [Å] at 295 K are also indicated (typical esds are 0.002 Å).

Electrostatic interactions: The appearance of these short O···C distances in crystals of carbonyl compounds had already been noted and discussed,[31–34] but their interpretation is still not clear. Standard arguments invoke electrostatic interactions between atoms of different electronegativity or favorably oriented dipoles. In such a line of thought the molecular arrangement in Figure 3 is largely dictated by, broadly speaking, a drive for the negatively charged carbonyl oxygens to reach for positively charged carbonyl carbon sites. Assuming these to be the key features of the crystal packing, one may understand the preferential use of screw axes in packing and hence the choice of the space group, since they can be obtained only by nonparallel molecular arrangements.

To further investigate the nature of these intermolecular interactions, the electrostatic interaction energies between the molecule and its neighbors in the crystal were calculated. The method[35] uses a 6-31G** wavefunction to calculate the electron density, and involves direct summation of nucleus–nucleus, nucleus–electron density, and electron density–electron density coulombic terms. A typical value for the elementary volume in the electron density calculation was $V = 0.001$ Å^3 with some 10^7 terms in the third term of the summation. The results in Figure 4 reveal that there is a very strong electrostatic stabilizing interaction with the S_y, S_z, and T_x molecular pairs (see the numerical data in Table 4). The S_x molecular pair is in close contact but contributes much less stabilizing energy. The O···C electrostatic stabilization in this case must be countered by significant repulsion between other sectors of the electron density, broadly corresponding to O···O and C···C contacts. Somewhat surprising is the appearance of many moderately destabilizing ($E_{int} > 0$) molecule–molecule interactions. Since the three closest molecular interactions amount to roughly 25% of the total sublimation energy, the overall picture that emerges from Figure 4 is one in which the succinic anhydride crystal is built on strong electrostatic stabilizing interactions with very few first nearest-neighbors, the rest of the structure adapting to accommodate this. The accurate experimental determination of some of the relevant intermolecular distances (Table 1) shows that there is no difference in temperature dependence between supposedly "attractive" (C···O) and supposedly "repulsive" (O···O) intermolecular distances; the repulsive nature of O···O contacts at distances of less than about 3.4 Å was demonstrated by careful calculations and experimental analyses by Leiserowitz et al.[36] The analysis of our 100-K diffraction data to extract atomic charges and dipoles is considered for future work.

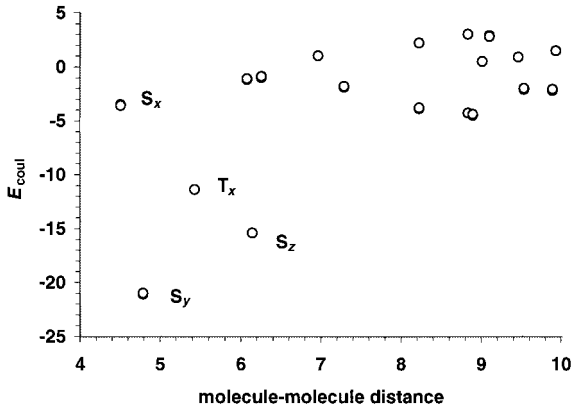

Figure 4. Molecule–molecule coulombic potential energies [kJ mol^{-1}] as a function of distance [Å] between centers of mass in the succinic anhydride crystal. The labels define the symmetry operator.

Perusal of Figure 4, moreover, reveals that the distance between molecular centers of mass does not correlate with electrostatic stabilization, and that significantly stabilizing electrostatic interactions also occur for molecules that are further apart, without any significant shortening of atom–atom distances and without any apparent special intermolecular arrangement. The interaction between translation-related molecules, whose dipoles must be parallel and of the same orientation by definition, may also be stabilizing from the electrostatic viewpoint, and Table 4 shows that there are no head-to-tail dipoles in the crystal of a highly polar molecule like succinic anhydride, because the angles between the mean molecular planes of screw-related molecules are always far from 0 or 180°.

The succinic anhydride crystal is high melting and stable. The expected heat of sublimation for its molecular dimensions[32] is 71 kJ mol^{-1}, much smaller than the actual experimental value. The results of the electrostatic calculations offer an explanation for the unusually high attractive forces in this crystal. At the same time, the discussion illustrates the dangers of crystal structure analysis based on singled-out atom–atom interactions, parallel versus antiparallel dipoles, or correlations between atom–atom distances and energy stabilization. Labeling certain atom–atom contacts as the cause, rather than a consequence, of crystal packing is always a subjective exercise. For a robust and significant discussion of intermolecular interactions, a quantitative assessment of all energetic factors is required.

Molecular dynamics simulations: Figure 5 shows the X-ray and MD results for the molar volume of succinic anhydride as a function of temperature, or the state equation of the material. Numerical data are collected in Table 5. The calculated crystal density at 295 K matches the experimental one by calibration, but differences never exceed 1.5% in the

  0947-6539/02/0807-1714 $ 20.00+.50/0 *Chem. Eur. J.* **2002**, *8*, No. 7

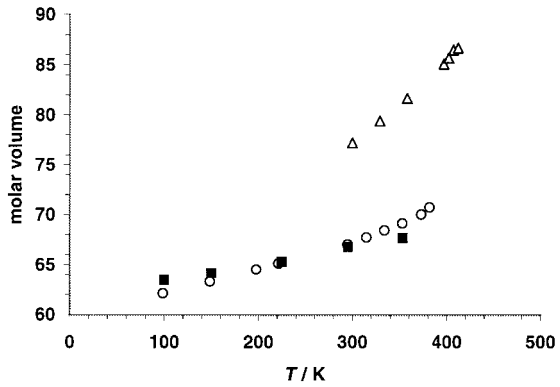

Figure 5. Molar volume [cm³] versus temperature for succinic anhydride. ■ crystal, experimental; ○ crystal and △ liquid, calculated from MD simulations.

Table 5. Results of molecular dynamics simulations. Energies in kJ mol^{-1}. In parentheses: rms fluctuations.

T [K]	V_{box} [Å^3]	ρ [g cm^{-3}]	E_{coul}	E_{vdW}	$\Delta H_{subl/vap}$
crystal					
100(2)	24.76(2)	1.611	−27.2	−61.1	91.0
149(2)	25.22(3)	1.582	−26.4	−59.2	88.2
222(3)	25.94(5)	1.538	−25.0	−56.4	83.9
295(4)	26.71(10)	1.493	−23.5	−53.7	79.6
353(4)	27.56(10)	1.447	−22.0	−50.9	75.2
liquid					
300(4)	30.75(18)	1.224	−15.6	−43.4	60.8
329(4)	31.65(21)	1.260	−14.9	−41.6	58.2
358(4)	32.58(25)	1.297	−14.2	−39.8	55.7

whole temperature range. The experimental isotropic thermal expansion coefficient is $1/V(\mathrm{d}V/\mathrm{d}T) = 2.6 \times 10^{-4}\,\mathrm{K}^{-1}$, quite in line with the average value for organic compounds (a study[37] of the distribution of such coefficients, taken from a survey of variable-temperature crystal structure determinations in the CSD, gives an average value of $2\,\mathrm{K}^{-1}$ for a spread from 1 to $4\,\mathrm{K}^{-1}$). The calculated value of $4.4 \times 10^{-4}\,\mathrm{K}^{-1}$ is somewhat larger, consistent with the large change in heat of sublimation with temperature, which exceeds that expected on the basis of the experimental $\Delta C_p(298\,\mathrm{K})$. For the liquid, we predict a thermal expansion coefficient of $1.0 \times 10^{-3}\,\mathrm{K}^{-1}$ and an enthalpy of vaporization of 61 kJ mol^{-1} at 300 K. These are reliable predictions of thermophysical quantities that are difficult to obtain experimentally.

The force field for succinic anhydride was derived by one-parameter rescaling of static atom–atom curves, with the addition of coulombic terms. To test the transferability of this optimized force field, we performed an MD simulation at 298 K for maleic anhydride, a very similar molecule whose crystal structure is strictly isomorphous to that of succinic anhydride. Parameters were the same as in Table 2 with a ± 0.10 electron charge separation over the CH groups. Results were: density: calculated 1.56, experimental 1.50 g cm^{-3}; sublimation energy: calculated 76, experimental 71 kJ mol^{-1}. Thus, even for a nearly identical molecule and an identical crystal structure, the discrepancies were 4 and 7%, respectively. Although tolerable in the context of a general purpose force field for static calculations, these deviations are such that the simulation of more subtle quantities, such as the melting temperature, would be hopelessly inaccurate.

Our conclusion here is that for the dynamic simulation of phase transitions in organic condensed phases, separate optimization of the force field for each molecule against available experimental data is indispensable. Given present-day computing facilities, the technical task is easy. However, more widespread and more accurate thermochemical data are needed for calibration.

For the solid–liquid transition, Figure 6 shows the MD trajectory for the crystal density as a function of temperature and simulation time. The calculated volume change at the melting temperature (387 K) is 19%, in line with normal

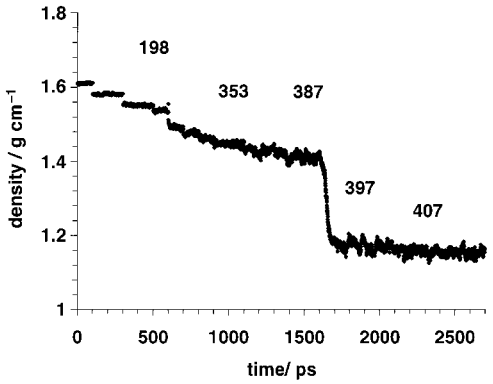

Figure 6. Evolution of density during the MD simulation of (left to right) the crystal, the melting transition, and the liquid. Temperatures are also shown.

values for organic crystals.[38] The liquid box obtained from fusion was then cooled in subsequent MD simulations, and this yielded estimates for the energy and density of the supercooled liquid down to room temperature; for obvious reasons (smallness of the computational box, short duration of the MD run) crystallization was not observed in the calculations. These results allow the estimation of the enthalpy of melting at room temperature, calculated as the difference in total energy of the liquid and the solid (the $P\Delta V$ term was neglected) to be 19.6 kJ mol^{-1}, in good agreement with the value obtained by combining the heat of formation of the liquid[39] with data in refs. [23, 24]. Figure 7 shows energy profiles over the melting event; apparently, the percentage losses in coulombic and dispersion energy are the same.

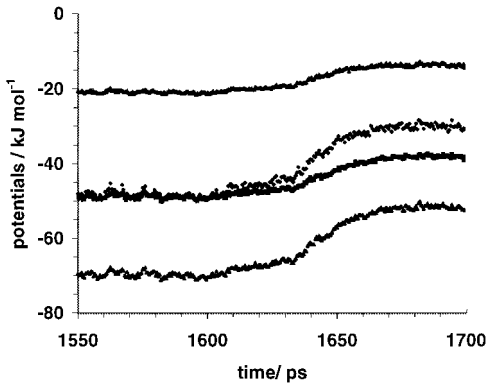

Figure 7. Energy breakdown over the melting event in Figure 6. Top to bottom: coulombic intermolecular, total (intra- and intermolecular), van der Waals, and total intermolecular potential energies.

The force field thus correctly reproduces crystal density, enthalpy of melting and of sublimation, and, within the limits of the simulation (see the discussion below), also the melting temperature. Test simulations conducted with small changes in charge parameters (-0.30 and -0.40 electrons for O atoms, $+0.55$ for carbonyl C atoms) resulted in a density at 295 K that was 4% too high, sufficient to raise the calculated melting temperature well above 450 K. This theoretical experiment confirms that very small density differences can have very large consequences for crystal stability, as already noted.[40]

The solid–liquid transition was also analyzed with regard to its structural and kinetic features. The density trajectory in Figure 6 shows that simulated crystal melting occurs more readily at 387 K than at lower temperatures. This is the most we can claim about the reproduction of the real melting temperature (392 K) by our force-field parameterization. The trajectory shows an abrupt transition, over a time span of less than 50 ps, from a moderately rotationally disordered crystalline state to a fully isotropic liquid state. One could question the significance of such nonequilibrium molecular dynamics simulations: strictly speaking, our run at 387 K is not dissimilar from an equilibration run for the liquid, which happens to start from an almost crystalline material. The proper way of analyzing the solid–liquid equilibrium would be to find the temperature at which the system, simulated for a sufficiently long time, would show random oscillations between the liquid and solid states. For obvious reasons of timescale, such a simulation is far beyond the realms of possibility. One must then be satisfied with a nonequilibrium, one-pathway glimpse at the phase space between liquid and solid, which the simulation at 387 K in fact is, and look for purely kinetic indications of what molecules may or may not want to do just before or during the phase transition.

For a detailed analysis of the rotational and translational molecular motions, a special MD run was carried out at 387 K, writing trajectories every 0.5 ps. Three rotational axes were defined, one passing through the carbonyl O atoms (approximately coincident with L1, Figure 2b), one through the ether O atom and the midpoint of the C–C bond (approximately coincident with L2, Figure 2b), while the third is the vector product of the first two. With $\boldsymbol{u}$ as the unit vector along any of these axes, three corresponding rotational correlation functions over the sample of N molecules in the box were calculated as Equation (1),[41]

$$C(i) = \Sigma_k \boldsymbol{u}(k,t)_i \boldsymbol{u}(k,0)_i / N \qquad (1)$$

where $i =$ L1, L2, L3; k runs over molecules in the computational box ($N = 240$); and each term in the summation is the cosine of the angle formed by each vector at time t to the corresponding reference vector at $t = 0$ (here chosen as that in the 100-K run). Translation was described by the three cartesian orthogonal components of displacement vector $\boldsymbol{d}$ of the center of coordinates, also with respect to standards at 100 K; the corresponding root-mean-square displacement functions are given by Equation (2).

$$T(i) = \left[\sum_k \{\boldsymbol{d}(k,t)_i - \boldsymbol{d}(k,0)_i\}^2 / N\right]^{1/2} \qquad (i = x, y, z) \qquad (2)$$

The $C(i)$ traces over the melting event are shown in Figure 8. All three $C(i)$ start from very near 0.9, that is, a minor loss of rotational correlation due to thermal libration, and after melting very quickly drop to zero, as expected for a pure isotropic liquid. Once the liquid phase is reached,

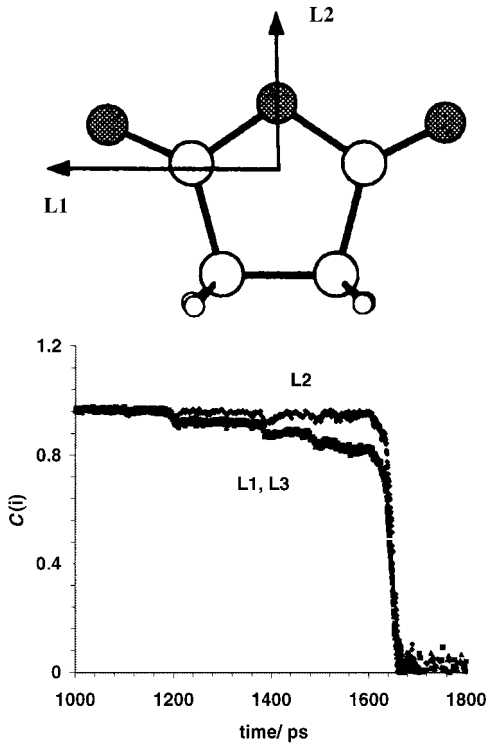

Figure 8. Rotational correlation functions for the rotation axes L1–L3 over the melting transition. L3 is perpendicular to L1 and L2.

calculated rotational correlation times were about 10 ps, as is appropriate for liquid organic substances.[41] In partial agreement with the analysis of ADPs in the crystal structure, Figure 8 shows that the "roll" molecular rotation (the L2 axis) is more hindered than the other two, since $C(2)$ remains higher than $C(1)$ or $C(3)$ up to the melting transition. Traces for the corresponding $T(i)$ functions show the absence of significant translational diffusion up to the melting transition.

What triggers the melting transition? In a naive perspective, the increased thermal energy pushes molecules further and further apart, until rotational and then translational diffusion set in and the crystal collapses. In our simulations, rotational diffusion sets in well below the melting point. A rotational diffusion event is defined here as one of the terms in Equation (1) becoming less than zero (a rotation of more than 90°). As Figure 9 shows, a number of such events already occur some 15 K below the melting temperature. Melting takes place when about 10% of the molecules show rotational diffusion around L2 or L3 (Figure 8), while rotation around L1 is restricted up until the very melting transition. (In the liquid, the number of such rotations averages to 120, or half the number of molecules in the computational box.) These pre-melting jumps purely draw from the thermal energy pool, and there is no hint of structural phase transitions close to the melting point in the

  0947-6539/02/0807-1716 $ 20.00+.50/0 *Chem. Eur. J.* **2002**, *8*, No. 7

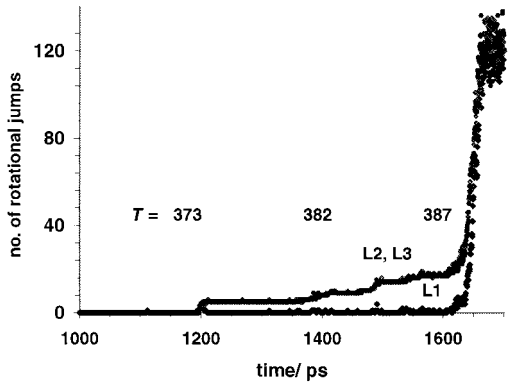

Figure 9. Number of rotational jumps in the 240-molecule crystal box over the melting event. Axis labels in Figure 8.

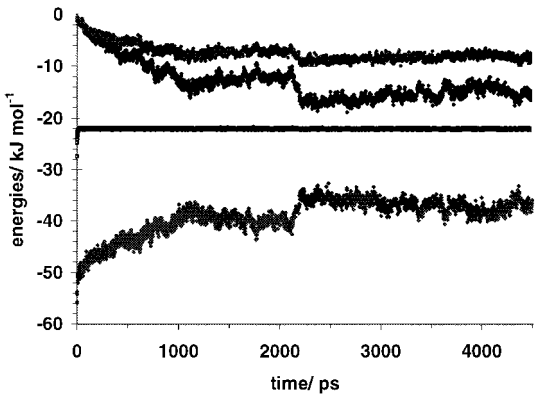

Figure 10. Evolution and breakdown of cohesive energies during the simulation of demixing in a solution box with 50 solute and 2145 solvent molecules. Top to bottom: solute–solute coulombic and van der Waals, solvent–solvent, and solute–solvent cohesive energies. The structural origin of the discontinuity at $t = 2200$ ps is unknown.

total energy trajectory of our simulations. This is in agreement with the absence of pre-melting features in the DSC trace.

Finally, the solvation, demixing, and nucleation processes were investigated as far as possible. A large number of molecular dynamics simulations were conducted starting from bimolecular or trimolecular aggregates extracted from the crystal (e.g., as in Figure 3), and solvated in a CCl_4 box. None of these oligomers survived the input of kinetic energy for more than a few picoseconds at or around room temperature. Although the molecule–molecule cohesive energies may be much larger than kT (see Table 4 and Figure 4), there are easy stepwise kinetic paths for climbing the dissociation energy barriers, and data in Table 4 confirm that many different molecular arrangements can be accessed at the expense of a few kilojoules per mole. Some dimers showed a propensity to remain bound for some time, the two partners tumbling one around the other, but the interaction geometry observed in the crystal was invariably destroyed almost immediately. These computational experiments further demonstrate that a correlation between small molecular aggregates in solution and molecular motifs in the crystal may not exist, even for a molecule that can use a strong electrostatic interaction for molecular recognition purposes. Similarly, oligomers of carboxylic acids were seen[12] to be relatively stable and bound in solution in nonpolar solvents, although hydrogen-bond breaking and transitions from dimer to catemer structures were frequent.

Dynamic aggregation studies with a larger number of solutes correctly reproduce the experimental fact that succinic anhydride readily demixes from weakly polar solvents (e.g., chloroform). Figure 10 shows the progress of demixing within the 50-molecule solution computational box, as shown by the steady increase in solute–solute cohesion at the expense of solute–solvent stabilizing interactions. In a few nanoseconds almost complete segregation of the solute is reached. The resulting molecular agglomerates seem to be stable at the size of 10–20 molecules, although they are of course completely liquidlike and fluxional, without a trace of crystalline order.

Conclusion and Perspective

Temperature-dependent X-ray diffraction analysis coupled with molecular dynamics simulation allow molecular interaction and molecular recognition phenomena to be studied, from macroscopic properties, such as expansion coefficients or phase transition enthalpies, to molecular level properties like the number and type of rotational defects in a melting material. For such simulations, the empirical force field approach is the only viable one, since ab initio quantum chemical or DFT methods are not cost-effective and suffer from basic inadequacies. For the study of subtler phenomena, however, the force field should be accurately calibrated for each compound, although with an eye to economy in the number of parameters. Transferability seems to be a requirement of the past.

On the experimental side, for better insight one would need a study of X-ray thermal diffuse scattering, and more sophisticated spectroscopic experiments, such as neutron inelastic scattering and the like, to probe the crystal dynamics. On the computational side, the ultimate goal is the simulation of a complete path from pure liquid or solution to crystalline solid with a view of the first steps in the formation of crystalline nuclei. Bridging the size and timescale gap is not yet feasible. Besides the obvious requirement of more computing power, one would perhaps need strategic protocols for control of temperature, pressure, and concentration gradients during the simulation. We believe that such studies are well within the maintstream of the physical chemistry of years to come.

Acknowledgement

We thank Dr. Lucia Carlucci for the DSC measurements and for the X-ray powder patterns.

[1] a) F. H. Allen, S. Bellard, M. D. Brice, B. A. Cartwright, A. Doubleday, H. Higgs, T. Hummelink, B. G. Hummelink-Peters, O. Kennard, W. D. S. Motherwell, J. Rodgers, D. G. Watson, *Acta Crystallogr. Sect. B* **1979**, *35*, 2331; b) F. H. Allen, O. Kennard, *Chem. Des. Automat. News* **1993**, *8*, 31.

[2] a) H. -B-Bürgi, S. Capelli, *Acta Crystallogr. Sect. A* **2000**, *56*, 403; b) S. Capelli, M. Fortsch, H.-B. Bürgi, *Acta Crystallogr. Sect. A* **2000**, *56*,

413; c) H. -B. Bürgi, S. C. Capelli, H. Birkedal, *Acta Crystallogr. Sect. A* **2000**, *A56*, 425.
[3] a) R. G. Della Valle, E. Venuti, A. Brillante, *Chem. Phys.* **1995**, *198*, 79; b) R. G. Della Valle, E. Venuti, A. Brillante, *Chem. Phys.* **1996**, *202*, 231.
[4] B. P. van Eijck, *J. Comput. Chem.* **2001**, *22*, 816.
[5] D. C. Sorescu, B. M. Rice, D. L. Thompson, *J. Phys. Chem. B* **1997**, *101*, 798.
[6] A. Gavezzotti, G. Filippini, *Chem. Commun.* **1998**, 287.
[7] A. Gavezzotti, *J. Mol. Struct. Theochem.* **2000**, *486*, 485.
[8] S. Devani, J. Anwar, *J. Chem. Phys.* **1996**, *105*, 3215.
[9] M. S. Westwell, M. S. Searle, D. H. Williams, *J. Molecular Recognition* **1996**, *9*, 88.
[10] A. Gavezzotti, *J. Chem. Soc. Perkin 2* **1995**, 1399.
[11] J. Anwar, P. K. Boateng, *J. Am. Chem. Soc.* **1998**, *120*, 9600.
[12] A. Gavezzotti, *Chem. Eur. J.* **1999**, *5*, 567.
[13] A. Altomare, G. Cascarano, C. Giacovazzo, A. Guagliardi, M. C. Burla, G. Polidori, M. Camalli, *J. Appl. Crystallogr.* **1994**, *27*, 435.
[14] G. M. Sheldrick, SHELX97, Program for crystal structure refinement, University of Göttingen, Germany, **1997**.
[15] A. L. Spek, *Acta Crystallogr. Sect. A* **1990**, *46*, C34
[16] L. J. Farrugia, *J. Appl. Crystallogr.* **1999**, *32*, 837.
[17] W. R. P. Scott, P. H. Hunenberger, I. G. Tironi, A. E. Mark, S. R. Billeter, J. Fennen, A. E. Torda, T. Huber, P. Kruger, W. F. van Gunsteren, *J. Phys. Chem. A* **1999**, *103*, 3596.
[18] W. F. van Gunsteren, S. R. Billeter, A. A. Eising, P. H. Hunenberger, P. Kruger, A. E. Mark, W. R. P. Scott, I. G. Tironi, Biomolecular Simulation: The GROMOS96 Manual and User Guide, BIOMOS b.v., Zürich-Groningen, **1996**.
[19] W. L. Jorgensen, D. S. Maxwell, J. Tirado-Rives, *J. Am. Chem. Soc.* **1996**, *118*, 11225.
[20] D. J. Price, J. D. Roberts, W. L. Jorgensen, *J. Am. Chem. Soc.* **1998**, *120*, 9672.
[21] G. Filippini, A. Gavezzotti, *Acta Crystallogr. Sect. B* **1993**, *49*, 868.
[22] A. Gavezzotti, G. Filippini, *J. Chem. Phys.* **1994**, *98*, 4831.
[23] Y. M. Yan, G. Pilcher, *J. Chem. Thermod.* **1990**, *22*, 893.
[24] H. G. M. De Wit, J. C. van Miltenburg, C. G. De Kruif, *J. Chem. Thermod.* **1983**, *15*, 651.
[25] I. G. Tironi, R. Sperb, P. E. Smith, W. F. van Gunsteren, *J. Chem. Phys.* **1995**, *102*, 5451.
[26] D. E. Williams, PCK83, QCPE Program 548, Quantum Chemistry Program Exchange, Indiana University, Bloomington, Indiana, **1983**.
[27] J. E. Coon, S. Gupta, E. McLaughlin, *Chem. Phys.* **1987**, *113*, 43.
[28] M. Ehrenberg, *Acta Crystallogr.* **1965**, *19*, 698.
[29] ORTEP: C. K. Johnson, ORTEPII: A Fortran Thermal Ellipsoids Plot Program for Crystal Structure Illustrations, Report ORNL-5138, Oak Ridge National Laboratory, Oak Ridge, **1976**.
[30] Gaussian: M. J. Frisch, G. W. Trucks, H. B. Schlegel, G. E. Scuseria, M. A. Robb, J. R. Cheeseman, V. G. Zakrzewski, J. A. Montgomery, Jr., R. E. Stratmann, J. C. Burant, S. Dapprich, J. M. Millam, A. D. Daniels, K. N. Kudin, M. C. Strain, O. Farkas, J. Tomasi, V. Barone, M. Cossi, R. Cammi, B. Mennucci, C. Pomelli, C. Adamo, S. Clifford, J. Ochterski, G. A. Petersson, P. Y. Ayala, Q. Cui, K. Morokuma, D. K. Malick, A. D. Rabuck, K. Raghavachari, J. B. Foresman, J. Cioslowski, J. V. Ortiz, A. G. Baboul, B. B. Stefanov, G. Liu, A. Liashenko, P. Piskorz, I. Komaromi, R. Gomperts, R. L. Martin, D. J. Fox, T. Keith, M. A. Al-Laham, C. Y. Peng, A. Nanayakkara, C. Gonzalez, M. Challacombe, P. M. W. Gill, B. Johnson, W. Chen, M. W. Wong, J. L. Andres, C. Gonzalez, M. Head-Gordon, E. S. Replogle, J. A. Pople, Gaussian 98, Revision A. 7, Gaussian, Inc., Pittsburgh PA, **1998**.
[31] H.-B. Bürgi, J. D. Dunitz, E. Shefter, *Acta Crystallogr. Sect. B* **1974**, *30*, 1517.
[32] A. Gavezzotti, *J. Chem. Phys.* **1990**, *94*, 4319.
[33] F. H. Allen, C. A. Baalham, J. P. M. Lommerse, P. R. Raithby, *Acta Crystallogr. Sect. B* **1998**, *54*, 320.
[34] V. Bertolasi, P. Gilli, V. Ferretti, G. Gilli, *New J. Chem.* **2001**, *25*, 408.
[35] A. Gavezzotti, *J. Phys. Chem.*, submitted.
[36] a) L. Leiserowitz, *Acta Crystallogr. Sect. B* **1976**, *32*, 775; b) Z. Berkovitch-Yellin, L. Leiserowitz, *J. Am. Chem. Soc.* **1982**, *104*, 4052.
[37] G. Filippini, personal communication.
[38] A. R. Ubbelohde, *The Molten State of Matter*, Wiley, Chichester, **1978**.
[39] E. S. Domalski, E. D. Hearing, *J. Phys. Chem. Ref. Data* **1993**, *22*, 964.
[40] A. Gavezzotti, *J. Am. Chem. Soc.* **2000**, *122*, 10724.
[41] J. D. Geerlings, C. A. G. O. Varma, M. C. van Hemert, *J. Phys. Chem.* **2000**, *B104*, 56.

Received: October 12, 2001 [F3607]

  0947-6539/02/0807-1718 $ 20.00+.50/0